International Journal of Hydrogen Energy 275 (2026) 157496

Contents lists available at ScienceDirect

International Journal of Hydrogen Energy

journal homepage: www.elsevier.com/locate/he

Off-grid electrochemical nitrogen reduction to ammonia I: Optimal design and operation

Michael J. Rix [a], Judith M. Schwindling [a], Karim Bidaoui [a], Alexander Mitsos [b,a,c,*]

[a] Process Systems Engineering (AVT.SVT), RWTH Aachen University, 52074 Aachen, Germany
[b] JARA-ENERGY, 52056 Aachen, Germany
[c] Energy Systems Engineering (ICE-1), Forschungszentrum Jülich, 52425 Jülich, Germany

ARTICLE INFO

Keywords:
Green ammonia
eNRR
Power-to-X
Flexible operation
Ammonia synthesis
Design and scheduling optimization

ABSTRACT

Electrochemical nitrogen reduction to ammonia (eNRR) promises green ammonia production with lower energy demand than the electrified Haber–Bosch process with water electrolysis (EHB) and the capability to operate on intermittent renewable electricity sources (RES). We evaluate the potential of eNRR by optimizing its design and operation with intermittent RES. Although the eNRR electrolyzer can adapt to fluctuations in electricity availability, nitrogen supply and ammonia purification are less flexible, constraining overall process flexibility. This limited flexibility requires costly battery storage and oversizing of renewable electricity supply. Consequently, even with optimistic eNRR performance, production costs exceed those of the EHB by more than 37 % due to a higher energy demand, larger electrolyzer, and less flexible separation processes. The coupling of storage capacity and discharge power of batteries result in costly and unfavorable battery utilization. These findings motivate assessing how alternative energy storage technologies can reduce production costs (part II).

1. Introduction

Ammonia is one of the most produced chemicals worldwide and is produced mainly via the Haber–Bosch (HB) process from nitrogen and hydrogen [1,2]. Hydrogen stems from steam methane reforming or coal gasification, resulting in high greenhouse gas (GHG) emissions. This motivates green ammonia, i.e., ammonia produced using renewable electricity. In addition to its conventional use for fertilizers and chemicals, green ammonia has the potential to be a promising energy carrier [3,4].

MacFarlane et al. [4] argue in their ammonia roadmap that green ammonia will be an important part of the future energy system and that "Generation 3" technologies that do not rely on the HB process will become industrially viable in the future. The HB process requires high temperatures and pressures and large production scales while Generation 3 technologies can potentially be operated under near-ambient conditions. Recent techno-economic analyses and reviews build on that and assess and compare different processes for the production of green ammonia, e.g., [5–10]. However, from these comparisons based on simple models, it remains unclear which emerging Generation 3 ammonia production technology will be the most promising due to their low technology readiness level (TRL) and development potential.

In this work, we focus on the electrochemical nitrogen reduction reaction (eNRR), one of the Generation 3 technologies. We assess the competitiveness of the eNRR for green ammonia production from intermittent green electricity by comparing it to the electrified Haber–Bosch process (EHB) with water electrolysis for hydrogen supply. The EHB is the most mature green ammonia technology. The reader is referred to the articles cited above for the comparison of different emerging ammonia production technologies.

Three reactions take place in the eNRR process. Ammonia is produced from water and nitrogen at the cathode via the eNRR [11]. The reaction is usually operated at near-ambient conditions. The side product hydrogen is produced via the competing hydrogen evolution reaction (HER). Other side reactions, such as the formation of hydrazine, are negligible [12]. The cathode catalyst and operating conditions must be tuned to increase the ammonia selectivity (also termed "Faradaic efficiency") and the reaction rate. Oxygen is formed as a by-product at the anode via the oxygen evolution reaction (OER) to close the charge balance.

$$\text{eNRR:} \quad N_2 + 6\,H_2O + 6\,e^- \rightleftharpoons 2\,NH_3 + 6\,OH^- \tag{1}$$

$$\text{HER:} \quad 2\,H_2O + 2\,e^- \rightleftharpoons H_2 + 2\,OH^- \tag{2}$$

$$\text{OER:} \quad 2\,H_2O + O_2 + 4\,e^- \rightleftharpoons 4\,OH^- \tag{3}$$

Currently, the eNRR suffers from low current densities and Faradaic efficiencies. For a comprehensive discussion on the current state of

* Corresponding author at: Process Systems Engineering (AVT.SVT), RWTH Aachen University, 52074 Aachen, Germany.
E-mail address: amitsos@alum.mit.edu (A. Mitsos).

https://doi.org/10.1016/j.ijhydene.2026.157496
Received 5 June 2026; Received in revised form 4 September 2026; Accepted 7 September 2026
Available online 16 September 2026
0360-3199/© 2026 The Authors. Published by Elsevier Ltd on behalf of Hydrogen Energy Publications LLC. This is an open access article under the CC BY license (http://creativecommons.org/licenses/by/4.0/).
Open access funding enabled and organized by Projekt DEAL.

catalyst development and process development for the eNRR reaction, the reader is referred to recent reviews, e.g., [11,12]. Several techno-economic analyses showed the potential of the eNRR process if considerable improvements in catalyst performance are achieved [6,7,9,13]. Recently, we identified catalyst performance targets for eNRR to be competitive with EHB for steady-state operation [14]. We showed that current catalyst performance levels are orders of magnitude below the identified targets. However, if these optimistic performance targets are met, the eNRR can be a competitive alternative to the EHB.

In the literature, the eNRR is considered to have several advantages compared to the EHB. First, the minimal energy demand of the eNRR is lower than that of the EHB, which makes it potentially more energy efficient. Second, its capital intensity can be lower because the eNRR operates under near ambient conditions and the high-temperature and high-pressure HB reactor is omitted, allowing for decentralized ammonia production [4,6,7,9,13]. Most importantly, the eNRR process is considered perfectly flexible: the eNRR electrolyzer can be cycled to zero load [4,6,7]. For example, Hochman et al. [7] investigated a grid-connected eNRR electrolyzer neglecting up- and downstream processes under fluctuating electricity prices and showed that flexible operation—turning the electrolyzer off at high electricity prices—reduced production costs.

However, this high flexibility and the ability to shut down the process apply only to the electrolyzer itself. Upstream and downstream processes for reactant supply and product purification may constrain flexible operation. Although these auxiliary processes typically have a much lower energy demand than the electrolyzer, some technologies cannot be ramped down to zero load. Consequently, the practical operability of a fully flexible eNRR process is constrained by the characteristics of these up- and downstream processes. To date, no study has investigated the coupling of eNRR with separation technologies under operation with intermittent electricity sources.

To address this gap, we investigate operation of an eNRR process with up- and downstream processes operated with RES. We consider solar power (SP) and wind power (WP) because of their globally unconstrained availability. SP and WP are intermittent in nature, their electricity production varies with time due to weather conditions. This intermittency can be accommodated via flexible operation and energy storage. We assess whether the theoretical advantages introduced above (lower energy demand, lower capital intensity, and greater flexibility) can be realized in a future eNRR process and whether the eNRR process can become a competitive alternative to the EHB.

First, we optimize the design and operation of an eNRR process coupled with intermittent electricity generation (part I). We optimize the sizing of the eNRR, up- and downstream processes, and SP and WP plants and the operation of each unit operation over one year to cancel out seasonality. We investigate different locations with different renewable electricity potentials. We consider optimistic future eNRR performance required for cost parity with the EHB for steady-state operation determined in our previous work [14]. Following this, we determine the influence of up- and downstream processes on flexible operation and production costs. The eNRR is compared to the EHB to determine if and how the eNRR can be competitive. Second, we consider advanced energy storage technologies that utilize available process streams to reduce production costs (part II [15]).

Such optimization of design scheduling has been conducted for the EHB (and other processes) in numerous studies, e.g., [16–22], but not for the eNRR. Recent reviews, such as Narciso et al. [23], give an overview of published studies and the underlying methodologies and assumptions.

The remainder of the manuscript is structured as follows. In Section 2, we introduce the investigated process, the investigated locations, the process model, and the formulation of the optimization problem. The results are presented in Section 3 and discussed in Section 4 and conclusions are drawn in Section 5.

2. Methods

The primary objective of modeling and optimization is to determine the optimal coupling between the electrolyzer, separation processes, and electricity supply associated with the lowest ammonia production costs. In addition, we introduce a model for the EHB process as a reference ammonia production process at higher TRL.

2.1. Process description

The eNRR process considered here consists of four process steps: reactant supply, electrochemical ammonia production, ammonia separation, and renewable energy system (cf. Fig. 1). The reactants, nitrogen and water, are supplied from an air separation unit (ASU) and water purification, respectively. Ammonia is produced in the eNRR electrolyzer and separated in the downstream separation step. All electricity is supplied from on-site WP and SP and the eNRR plant is not connected to an electrical grid. On-site renewable electricity generation ensures that all ammonia is produced only from additional renewable electricity capacity, which can be important to certify as green ammonia.

The generation of electricity from WP and SP is intermittent and therefore dependent on time. This time-dependent electricity supply requires dynamic operation of the eNRR process and/or large electricity storage. We consider three operating strategies of the energy system: (i) direct coupling of RES and eNRR plant, (ii) curtailment of excess electricity, and (iii) battery storage. In direct coupling, the eNRR plant must consume the electricity produced by the RES at all times. Curtailment allows for partial decoupling of electricity generation and consumption, and thus oversizing of electricity generation to increase off-peak availability. Battery storage allows for further decoupling of generation and consumption.

2.2. Process model

We model the eNRR process to determine the energy demand and cost of ammonia production. In the following, we derive quasi-steady-state models of the sub-processes introduced before. These models are then combined and optimized to determine the design and operation with the lowest production costs.

The availability of electricity from WP and SP varies with time. Thus, the eNRR process will not operate in steady state but with a time-varying electricity input and ammonia production rate. The resulting process model calculates the ammonia production rate and costs as a function of the sizes of the eNRR, SP, and WP plants and the time-varying power input. We consider the operation over a one-year time horizon to cancel out seasonal effects.

2.2.1. Dynamic vs. quasi-steady-state modeling

Operation with varying electricity prices, electricity availability, or product demand requires flexible, time-variable (dynamic) operation. In principle, this necessitates dynamic modeling of the process, often resulting in large and computationally expensive optimization problems when considering design and operation over extended time periods (weeks to years). To overcome this limitation and facilitate (global) optimization, quasi-steady-state operation is a common assumption in the design and scheduling optimization of energy and chemical processes. When the dynamic behavior of the investigated process is incorporated with appropriate ramp rates and load constraints, quasi-steady-state modeling can result in an accurate representation of the dynamic behavior [24].

Time-dependent models can be classified into continuous-time models in which the time-dependency is described by solving differential equations and into discrete-time models in which the time horizon is discretized into constant time intervals. In the latter, the system of ordinary differential equations is transformed into a system of algebraic equations, reducing the computational effort.

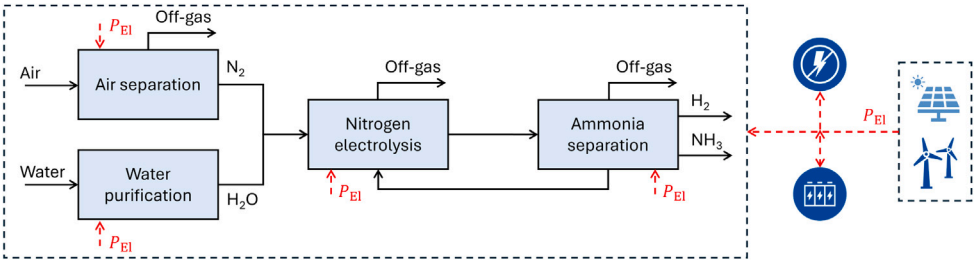


Fig. 1. Process block diagram for the eNRR process with renewable electricity supply from WP and SP and optional battery storage. Reactants are supplied from air separation and water purification; ammonia is produced in the electrolyzer and separated in the separation step.

We implement discrete-time quasi-steady-state models and discretize the time horizon into time series of constant operation. It is assumed that the system can adjust to a new input instantaneously and that the output is constant over the time interval. We introduce appropriate ramp rates and lower load limits to represent the dynamic behavior. This results in an accurate and computationally tractable model that allows the optimization of design and operation for the time period of one year.

This quasi-steady-state modeling (implicitly or explicitly) contains the assumption that the time constant of the system with respect to the applied load change is much smaller than the time discretization. Commonly, hourly discretization is chosen because electricity prices and renewable electricity availability are available at hourly resolution. The time scales of load changes of electrochemical processes are considerably smaller than the hourly resolution (e.g., [25] for PEM water electrolysis or [26] for chlorine). Therefore, the quasi-steady-state assumption is valid for electrochemical processes.

Other chemical processes respond much slower to load changes due to thermal and material inertia. In particular, cryogenic air separation processes can have response times in the order of a few hours [27]. Fahr et al. [28] showed via dynamic modeling that a HB process designed for flexible operation can achieve load changes up to 3 %/min.

Sass and Mitsos [24] argued that for such longer response times, a simple quasi-steady-state assumption is not valid. The larger time constants must be accounted for by introducing ramp rate constraints and lower load limits. These ramp rates reduce the maximum load change of the equipment, reflecting the larger time constants. In this work, we will employ a quasi-steady-state model with appropriate ramp rates and lower load limits for the unit operations with limited flexibility, such as the air separation unit.

2.2.2. Water purification

The eNRR process requires water as a proton source. The required water purity is not known due to the low TRL of the process. We assume that deionized water, similar to alkaline water electrolysis, is required [29]. Simoes at al. [30] estimated costs of supplying deionized water for electrochemical processes from different water sources. Considering the costs reported therein and a water usage efficiency of 50 %, the specific costs (investment and operation) of water purification are $0.028\,€\,kg_{NH3}^{-1}$.

Ghobeity and Mitsos [31] investigated the production of potable water from seawater via reverse osmosis with a quasi-steady-state model and allowed for turning off without ramp constraints. They argued that experimental validation (e.g., [32]) showed that response times are less than a minute. We assume that these results on flexible operation of seawater to potable can be transferred to seawater or potable to deionized.

As the specific costs for water purification ($\sim 0.028\,€\,kg_{NH3}^{-1}$) are considerably lower than the expected production costs of ammonia ($\sim 1\,€\,kg_{NH3}^{-1}$) and the response time is fast, we do not need to consider water purification within the scope of this study explicitly. The influence on the costs and energy demand is negligible, and the water purification does not impose constraints on the flexible operation of the eNRR process.

2.2.3. Nitrogen supply by air separation

Nitrogen can be supplied from cryogenic air separation, membrane separation, and pressure swing adsorption. Cryogenic air separation can achieve the highest purities, is suitable for large production rates, and has the lowest specific energy demand. However, the flexibility of cryogenic air separation is lower [33].

In a cryogenic air separation unit (ASU), air is split into its components. ASUs can have different layouts and produce different products; we model an ASU that produces only pure nitrogen as described, e.g., in [27]. Neither oxygen nor argon are required in the eNRR process; in fact oxygen is a also a byproduct of the electrolysis.

There has been considerable effort to increase the flexibility of cryogenic ASUs in recent years, highlighted in a review by Klein et al. [34]. We model the ASU based on a dynamic simulation and control study by Schulze et al. [35]. They calculated the specific energy demand for different part loads. After steady-state was reached, the specific energy demand was similar in all part loads. Thus, we calculate the ASU energy demand $P_{ASU,t}$ at each time step t from the nitrogen mass flow $\dot{m}_{N2,t}$,

$$P_{ASU,t} = p_{ASU} \cdot \dot{m}_{N2,t} \ , \tag{4}$$

assuming a constant specific energy demand p_{ASU}. The specific energy demand is given in the supporting information (SI).

Despite the recent progress in flexible ASU operation, the load range is limited and the response time of load changes is in the order of an hour [35]. We account for this by imposing ramp rate RR_{max} constraints (cf. Eqs. (5) and (6)) and a lower load limit LLL (cf. Eq. (7)). These flexibility limitations are estimates from literature and tested in a sensitivity analysis. Note that writing the ramp rates and lower load limit with respect to the power or mass flow is equivalent due to their linear correlation.

$$P_{ASU,t} - P_{ASU,t-1} \leq RR_{max} \cdot P_{ASU,max} \tag{5}$$

$$P_{ASU,t-1} - P_{ASU,t} \leq RR_{max} \cdot P_{ASU,max} \tag{6}$$

$$P_{ASU,t} \geq LLL \cdot P_{ASU,max} \tag{7}$$

We calculate the ASU investment cost $CAPEX_{ASU}$,

$$CAPEX_{ASU} = c_{ASU} \cdot \dot{m}_{N2,max} \ ,$$

assuming a linear relationship with plant capacity $\dot{m}_{N2,max}$. We neglect capacity-specific investment cost reductions with plant size (economies of scale). This assumption has limited influence on the results due to the low share of the ASU CAPEX in production costs.

The nominal capacity of the ASU $\dot{m}_{N2,max}$ (and all other equipment) is calculated from an inequality constraint:

$$\dot{m}_{N2,t} \leq \dot{m}_{N2,max} \ \forall t \ . \tag{8}$$

Larger plant capacities increase the objective function. Thus, the optimizer will always choose the lowest possible plant capacity that satisfies Eq. (8). This implementation avoids the discontinuous max function and is common practice in design and scheduling optimization.

The variable operating costs (OPEX) for electricity are accounted for by the energy balances at every time step. Fixed operating costs for

operation and maintenance $OPEX_{O\&M}$ are calculated from the CAPEX with the factor $f_{O\&M}$,

$$OPEX_{O\&M,ASU} = f_{O\&M,ASU} \cdot CAPEX_{ASU} \ . \quad (9)$$

Similar relationships to Eq. (9) will be applied for calculating costs for operation and maintenance for all equipment in this study.

We assume that the ASU has a liquid nitrogen tank with the capacity of one day of operation at nominal load (similar to [35]). The level in the storage tank is inherently dynamic. The nitrogen mass $m_{Tank,t}$ in the tank is calculated at every time step t by applying the forward Euler scheme (cf. Eq. (10)). $\dot{m}_{in,t-1}$ and $\dot{m}_{out,t-1}$ are the in- and outgoing flows, respectively, and Δt is the time discretization (1 h).

$$m_{Tank,t} = m_{Tank,t-1} + \dot{m}_{in,t-1} \cdot \Delta t - \dot{m}_{out,t-1} \cdot \Delta t \quad (10)$$

2.2.4. eNRR electrolyzer

The electrolyzer is modeled to calculate the production rate and costs as a function of electricity input and electrolyzer size. The reaction can take place in alkaline, neutral, or acidic conditions [11]. We consider an alkaline eNRR electrolyzer operating at near-ambient conditions and a finite-gap electrolyzer set-up with nitrogen supply via a gas diffusion electrode. Ammonia is produced from water and nitrogen (cf. Eq. (1)) at the cathode. The side product hydrogen is formed in the HER competing with the eNRR (cf. Eq. (2)) and the by-product oxygen at the anode (cf. Eq. (3)). For a more detailed description of the eNRR electrolyzer, the reader is referred to our previous publication [14] and recent eNRR literature [9,11,12].

The energy demand, efficiency, and current density (and thus reactor size) depend on the catalyst performance. The eNRR technology is still at a low TRL, and no catalyst with promising performance levels has been published today. Evaluating the current state of processes at such low TRL and performances far from commercial viability in a techno-economic analysis reveals little insight. Instead, such a study must evaluate future process performance to assess whether a process can achieve commercial viability and which process performance is required for this. In our previous study [14], we performed such an evaluation for the eNRR and calculate performance targets for cost parity with the EHB process for steady-state on-grid operation. These performance targets are a curve of required current density as a function of the Faradaic efficiency.

Nominal eNRR operation is modeled as one tuple of current density and Faradaic efficiency from this previous study. We utilize a Faradaic efficiency of 70 % and a nominal current density of 3410 $A\,m^{-2}$ as the base case for the main evaluation and study the influence of process performance by varying this point. This corresponds to a specific energy demand of 13.8 $kWh\,kg_{NH3}^{-1}$ for ammonia synthesis in the eNRR electrolyzer at the nominal operating point. This value only considers ammonia synthesis and not nitrogen supply and ammonia purification.

Part-load operation is modeled by reducing the current density and assuming that the Faradaic efficiency is constant. In reality, the Faradaic efficiency could increase or decrease during part-load operation, depending on the catalyst and process. However, this relationship cannot be described because of the lack of reliable experimental data. Assuming a certain reduction or increase of the Faradaic efficiency at reduced current densities would be arbitrary.

We assume that the eNRR electrolyzer can be operated ideally flexible, i.e., operation can be changed from nominal load to turned off and vice versa in two consecutive hours. In the literature, the eNRR is assumed to be more flexible than the EHB [6,7]. We make this assumption to assess whether this high flexibility of the eNRR electrolyzer translates into flexibility of the eNRR process and whether this flexibility is a strong competitive advantage compared to the EHB.

However, the specific energy demand changes during part-load operation. Losses in the electrolyzer stem from ohmic and activation overpotentials [36]. These overpotentials are reduced at lower current densities, resulting in higher efficiency and lower specific electricity demand at part-load operation. This lower specific electricity demand must be considered when modeling the part-load operation, resulting in a more complex relationship than for the ASU.

For implementation in the linear optimization model, we require a linear model that relates electrolyzer power and size to the ammonia production rate. Implementing a detailed electrolyzer model results in non-linear and implicit equations [36]. Even though libraries for detailed dynamic electrolyzer modeling are available (such as [37]), they are computationally too expensive for implementation in design and scheduling optimizations. We overcome this by deriving a detailed electrolyzer model and calculating electricity demand and ammonia production over the load range (0 % to 100 %) and fitting a piecewise affine approximation of the ammonia production rate to the power input of the electrolyzer. The electrolyzer model is detailed in the SI.

The relationship between electrolyzer power and production rate is a concave function that can be described well with a piecewise affine approximation (cf. Figure S1 in the SI). This piecewise approximation preserves the concave shape of the relationship and captures the increase in electrolyzer efficiency during part load in a linear model. However, the direct implementation of this piecewise affine approximation would result in a considerable number of integer variables for the considered time horizon of one year, as this approximation will be evaluated for every time step. To circumvent the computational effort associated with mixed-integer problems, we reformulate the problem as proposed by Varelmann et al. [38]. We reformulate every piecewise affine function as an inequality constraint,

$$\dot{m}_{NH3,t} \leq a_{0,i} + a_{1,i} \cdot P_{Elec,t} \quad \forall i \in \{1, \dots, n_{fit}\} \ , \quad (11)$$

with the parameters of the affine function $a_{0,i}$ and $a_{1,i}$ that are fitted to the full model. We do not keep track of the linearization interval and treat the inequalities as globally valid.

Nonphysically low ammonia production at a certain electricity input is feasible with this reformulation. The feasible set is enlarged from the affine functions to the area enclosed by the affine functions, the bounds of $\dot{m}_{NH3,t}$ and $P_{Elec,t}$, and the x-axis. However, as the optimization model considers both the cost of the electricity and the investment cost of the electrolyzer, such nonphysically low production rates would increase the specific electrolyzer investment costs, and as such, the objective value. Due to this, the optimization solver will always maximize ammonia production at a given electricity input. The ammonia production will always be on the respective active affine function.

This is visualized in Figure S1 in the SI. The affine function fitted on a specific interval is always the tightest approximation on this interval because of the concave nature of the approximated function. Therefore, the formulation is equivalent to the formulation with integers. The accuracy of the model is improved compared to the assumption of constant electrolyzer efficiency without sacrificing computational speed.

Such a reformulation can be applied to concave functions where higher values lower the objective function, as in this case, and as it is often observed in the part-load operation of flexible plants. This reformulation could also be applied to convex functions when lower function values decrease the objective function, i.e., problems that are mirrored compared to the one presented.

In the literature, no information on the CAPEX of an eNRR electrolyzer is known; this process has not been built so far. To overcome this, eNRR CAPEX are estimated from alkaline water electrolysis CAPEX. Alkaline water electrolysis is the most similar mature technology. Costs for water electrolyzers are commonly reported either relative to the nominal power (in € kW^{-1}) or relative to the electrolyzer area (in € m^{-2}). Some electrolyzer components scale with respect to the power, such as the power converter. In contrast, some components scale with respect to the electrolyzer area, such as the stacks. When calculating costs for a technology with a similar nominal power density ($kW\,m^{-2}$), both approaches are equal.

This is not the case for the eNRR. The nominal power density is not known at the current state of development; it depends on the catalyst performance and the nominal operation point of the electrolyzer. Therefore, we cannot simply transfer costs for water electrolyzer, and must account for differences in the technologies.

We transfer water electrolyzer costs by removing components of water electrolysis that are not needed in the eNRR (such as product gas compressors), adding additional components (such as the gas diffusion electrode), and by identifying which components scale with respect to the electrolyzer area A_{Elec} and which with respect to the electrolyzer power P_{Elec} (cf. Eq. (12)). The resulting relationship,

$$\mathrm{CAPEX}_{\mathrm{Elec}} = \left(c_{\mathrm{A}} \cdot A_{\mathrm{Elec}} + c_{\mathrm{P}} \cdot P_{\mathrm{Elec}}\right) \cdot f_{\mathrm{H}} \,, \tag{12}$$

describes electrolyzer $\mathrm{CAPEX}_{\mathrm{Elec}}$ as a function of the electrolyzer area and nominal power. Both the area and the nominal power result from the catalyst performance (nominal current density, Faradaic efficiency, and overpotentials) and the required ammonia production rate.

The cost coefficients c_{A} and c_{P} are calculated from a bottom-up water electrolyzer cost analysis by Holst et al. [39]. Their bottom-up approach allows us to exclude unnecessary equipment and to split the costs into power-dependent and area-dependent (cf. Table S1 in the SI). Their cost analysis includes only electrolyzer manufacturing and not installation. We account for additional costs such as overhead and engineering as proposed by Hemauer et al. [40] by multiplying CAPEX with a Hand factor f_{H}. We assume an electrolyzer lifetime of 10 years. Fixed OPEX for operation and maintenance are calculated by multiplying the investment costs by a factor $f_{\mathrm{O\&M}}$ (cf. Eq. (9)). The variable OPEX for electricity is accounted for by the energy demand of the electrolyzer and the investment costs of the SP and WP plants.

In deriving the electrolyzer model, we implicitly assume that the electrolyzer dynamics are fast and thus negligible compared to the hourly discretization. No ramp rates are applied. We assume no lower load limit and that the electrolyzer can be turned off. In alkaline water electrolysis, reverse currents degrading the catalyst can occur when the electrolyzer is turned off [41]. We assume that this can be circumvented for the presented technology. In addition, we assume that the HER is the only side reaction and that no shunt currents or other current losses occur.

2.2.5. Ammonia separation and purification

Ammonia is produced at the gas diffusion electrode, which is in contact with both the liquid electrolyte and the gaseous nitrogen stream. Consequently, ammonia may be present in both the liquid and gas phases. By separating ammonia from one phase while recirculating the other, the purification step can be limited to a single phase. Several technologies for ammonia separation from gas streams and aqueous solutions have been discussed in the literature.

Ammonia can be separated form the gas stream by absorption in ionic liquids [42]. Tailored ionic liquids may exhibit high ammonia solubility and low water solubility [43,44]. Ammonia absorption requires elevated pressure, desorption requires a slight vacuum, which increases the energy demand [42]. In addition, all studies considered absorption from dry gases. In humid gases, as present here, the low solubility of water could lead to water contamination in the product gas. Therefore, further studies on tailored ionic liquids for ammonia separation from humid gas streams are required before this technology can be considered a viable purification option. Membrane contactors have also been studied to absorb ammonia from gas mixtures into liquid solutions [45]. However, this still requires subsequent separation of ammonia from the liquid solution, for example by distillation. Finally, ammonia adsorption on solid sorbets requires elevated temperatures and pressures [46].

We consider the separation of a liquid mixture of ammonia and water by means of distillation. This allows for ammonia separation at the desired purity in one step. We assume that all net generated ammonia is in the liquid phase and that other components in the liquid phase, such as the dissolved gases and the electrolyte, do not substantially influence the separation.

The distillation column for purifying ammonia is modeled similarly to the ASU (Eqs. (4)–(7)). The energy demand at each time step $P_{\mathrm{Sep},t}$ is calculated from the ammonia production rate $\dot{m}_{\mathrm{NH3},t}$ and the specific energy demand p_{Sep}. The specific energy demand is calculated from an Aspen Plus simulation of the distillation column. We assume that the specific energy demand is constant in part-load operation. The limited flexibility is accounted for by employing a ramp rate and a lower load limit.

The distillation column and the electrolyzer are decoupled by a buffer tank. The buffer tank balance is calculated similarly to Eq. (10). The capacity of the buffer tank is an optimization variable.

Investment costs for the distillation column and buffer tanks are calculated from correlations by Turton et al. [47]; the calculations are detailed in the SI. We linearized the nonlinear cost correlations by calculating the tangent at the expected capacity. When the capacities determined by the optimization deviated considerably from the linearization point, we iteratively adjusted the linearization (cf. Figure S2 in the SI).

2.2.6. Renewable electricity model

The availability of electricity from WP and SP is modeled using the methods provided in [48,49] and data collected in [50]. Data on electricity generation are available at hourly resolution. We investigated three locations with different renewable electricity potentials: one location each with high WP and low SP potential, low WP and high SP potential, and high WP and high SP potential (cf. Table 1).

The electricity availability at each time step $P_{\mathrm{gen},t}$,

$$P_{\mathrm{gen},t} = \mathrm{CF}_{\mathrm{RES},t} \cdot P_{\mathrm{nom,RES}} \,,$$

is calculated from the tabulated capacity factor $\mathrm{CF}_{\mathrm{RES},t}$ and the installed capacity $P_{\mathrm{nom,RES}}$ (optimization variable).

We assume linear scaling of CAPEX and OPEX with installed capacity,

$$\mathrm{CAPEX}_{\mathrm{RES}} = c_{\mathrm{inv,RES}} \cdot P_{\mathrm{nom,RES}}$$
$$\mathrm{OPEX}_{\mathrm{O\&M,RES}} = c_{\mathrm{O\&M,RES}} \cdot P_{\mathrm{nom,RES}} \,,$$

due to the numbering up of WP and SP. The cost factors for investment $c_{\mathrm{inv,RES}}$ and operation and maintenance $c_{\mathrm{O\&M,RES}}$ are taken from recent cost reports by the US Department of Energy [51,52]. These cost factors represent installed costs.

2.2.7. Curtailment

We allow for electricity curtailment. SP cells can be disconnected, and WP turned out of the wind. By these means, the electricity production can be reduced below the one calculated from the installed capacity and the availability at the current time step.

Allowing for curtailment enables partial decoupling of electricity generation and consumption. The SP and WP plants can be oversized compared to the nominal load of the electrolyzer and curtailed when the availability exceeds the possible consumption of the electrolyzer and the other components. Due to this oversizing of SP and WP plants, the electricity availability at off-peak hours relative to the electrolyzer's nominal load can be increased, and the electrolyzer can operate at a higher load throughout the year.

2.2.8. Battery model

Battery storage allows for further decoupling of electricity production and consumption. Electricity stored at high availability can be consumed at low availability. Lithium-ion batteries for energy storage in scheduling optimizations are commonly modeled using linear power models. In a recent review, Vykhodtsev et al. [53] compared different battery model formulations. They state that the simplest "Power-Energy Model" that is applied in many studies due to its simplicity can lead to

Table 1
Investigated locations and mean capacity factor. The mean capacity factor is the mean load of the electricity generation over the year. Generated using [48–50].

	Latitude	Longitude	Mean capacity factor WP	Mean capacity factor SP
Denmark	56.226	8.168	57 %	13 %
Chile	−19.659	−70.033	3 %	23 %
Australia	−22.21	113.986	42 %	23 %

infeasible operation, especially when considering short-term operation and ancillary services. More complex models considering the chemistry of the battery and degradation result in a more accurate representation but introduce nonlinearities and/or integers.

In this work, we employ a linear battery model because of the lower computational effort as described by Vykhodtsev et al. [53] and the works cited therein. Potential uncertainties and errors from this simplified analysis will be small compared to the uncertainty in the eNRR processes and cost estimations. The model consists of an energy balance of the battery, constraints regarding the charging and discharging rate, and cost calculation.

The state of charge SoC_t of the battery corresponds to the amount of energy stored in the battery and is calculated from the battery energy balance,

$$SoC_t = SoC_{t-1} + P_{Char,t-1} \cdot \Delta t - P_{Dis,t-1} \cdot \Delta t \ ,$$

with the charging P_{Char} and discharging rates P_{Dis} and the time discretization Δt (1 h). The round-trip efficiency η_{RTE} is considered when including the discharging in the electricity balance. We constrain the upper and lower limits of the state of charge:

$$SoC_{min} \leq SoC_t \leq SoC_{max} \ .$$

For lithium-ion batteries, the maximal charging rate and the capacity of the battery are correlated. We assume that a battery with a capacity of four hours at the maximum charging rate is installed. Therefore, the charging and discharging rates are restricted by this maximum charging rate:

$$P_{Char,t} \leq \frac{SoC_{max} - SoC_{min}}{4\,h}$$
$$P_{Dis,t} \leq \frac{SoC_{max} - SoC_{min}}{4\,h} \ .$$

In the presented model, simultaneous charging and discharging may occur. This is a mathematical artifact that is often observed in the literature [53] when employing such a model for scheduling optimization of grid-connected batteries during periods with negative electricity prices. During these negative prices, simultaneous charging and discharging will "destroy" electricity (converted to heat due to irreversibilities) and thereby generate value.

In our model, there will be no negative electricity prices because we do not model electricity prices in the off-grid case (electricity costs are model with via OPEX and CAPEX for the WP and SP). What we observed, however, is battery discharge during times in which the electricity availability from WP and SP exceeds the electricity consumption of the plant, i.e., during times with curtailment. This stems from the same mathematical artifact. Discharging during periods with excess electricity does not change the outcome of the analysis as long as the battery is fully charged at the end of the high-availability period. This discharging only increases the amount of curtailment of WP and SP. Due to this, we do not prevent this phenomena.

OPEX and CAPEX are calculated from a linear relationship with battery capacity SoC_{max},

$$CAPEX_{Bat} = c_{inv,Bat} \cdot SoC_{max}$$
$$OPEX_{O\&M,Bat} = c_{O\&M,Bat} \cdot SoC_{max} \ .$$

Battery capacity is increased by numbering up; thus, we assume a linear correlation of costs. The cost factors for investment $c_{inv,Bat}$ and operation and maintenance $c_{O\&M,Bat}$ are taken from a recent report on utility-scale batteries by the US Department of Energy [54]. The costs are the overnight capital costs for the whole battery system, including purchasing and installation of all relevant units.

2.2.9. Material and energy balances

The individual units presented above are coupled by material and energy balances. The ammonia production in the electrolyzer $\dot{m}_{NH3,Elec,t}$ is linked to the nitrogen output from the ASU storage tank $\dot{m}_{N2,ASU,t}$,

$$\dot{m}_{NH3,Elec,t} = 0.5 \cdot \dot{m}_{N2,ASU,t} \cdot \frac{M_{N2}}{M_{NH3}} \ , \quad (13)$$

via the stoichiometry of the reaction and the molar masses. Similar relationships can be derived for hydrogen production and water consumption, which are not detailed here.

The electricity production and consumption of every unit are linked by the electricity balance.

$$P_{SP,t} + P_{WP,t} + P_{Dis,t} \cdot \eta_{RTE} = P_{ASU,t} + P_{Elec,t} + P_{Sep,t} + P_{Curt,t} + P_{Char,t} \quad (14)$$

2.2.10. Electrified Haber–Bosch process

Numerous studies on the design and operation of the EHB process with water electrolysis exist in the literature (see Narciso et al. [23] for a recent review). We model the EHB process to compare the eNRR and EHB based on similar assumptions. We consider an EHB process as shown in Fig. 2 consisting of water purification, PEM water electrolysis, cryogenic air separation, nitrogen and hydrogen compression, hydrogen storage, the HB reactor, and separation and purification of ammonia. All energy is supplied by on-site electricity production from WP and SP. We allow for electricity curtailment and employ battery storage.

Some unit operations of the EHB process are similar to the eNRR unit operations (cf. Fig. 1). Both require water purification and air separation for reactant supply. Both have an electrolyzer as the main energy consumer. The EHB requires additional compression and a high-pressure synthesis loop. However, ammonia separation and purification are simpler for the EHB because ammonia can be condensed from the gas mixture. In the eNRR, the gas mixture contains water that would condense first and freeze.

The unit operations also contained in the eNRR process are modeled as introduced above. We assume a perfectly flexible PEM electrolyzer with constant efficiency at part-load that can be turned off. The specific energy demand and the cost coefficients for CAPEX and OPEX are taken from Holst et al. [39], which was also the basis for the eNRR cost estimation. We add the same Hand factor [40] as for the eNRR electrolyzer to account for installation costs.

The energy demand at nominal load and cost for the HB synthesis loop consisting of compression, HB reactor, and ammonia purification are taken from Morgan et al. [55] and updated to 2023 using the CEPCI factor. The part-load operation is modeled based on Fahr et al. [28]. They modeled the dynamic operation of a load-flexible HB process and state that the load can be reduced down to 20 % with ramp rates of 3 %/min. However, they state that the energy demand of the HB loop can only be reduced to 50 % at minimal load due to the limited flexibility of the compressors in the refrigeration cycle (for ammonia separation). The flow through the compressors cannot be reduced too much to prevent entering the surge region. Therefore, large

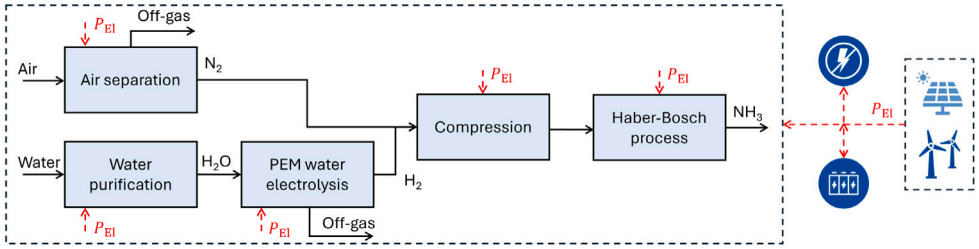


Fig. 2. Block diagram of the electrified Haber–Bosch process (EHB) with water electrolysis as considered in this study.

recycle streams are required for each compressor to keep the flow rates sufficiently high, resulting in a similar power demand in part and full load. We model the EHB power demand by assuming a linear reduction in energy demand and 50 % energy demand at minimal load, similar to the suggestion by Fahr et al. [28].

We assume that the PEM electrolyzer and hydrogen compressor can be operated flexibly without loss in efficiency. While the first is rather reasonable, the latter will have decreased efficiency at part load. However, the energy demand of the compressor is low in comparison to that of water electrolysis, and the compressor operates only when the electrolyzer is also in operation. When the electrolyzer is turned off, the HB process is operated with hydrogen from the high-pressure storage tank. Therefore, this simplification in the compressor modeling is expected to have little influence. The ASU is modeled with the same lower load limit and ramp rates as introduced above.

By formulating mass and energy balances, we derived a process model for the EHB. This model calculates the ammonia production at a given electricity input and sizing of the unit operations. The model structure and assumptions are similar to the eNRR. The EHB model serves as a benchmark process and is optimized for the same locations.

2.3. Formulation of the optimization problem

We optimize the design and operation of the eNRR electrolyzer for one-year operation. We minimize the total annualized cost of installing and operating the plant,

$$\min_{\mathbf{x},\mathbf{y}} \sum_i (\mathrm{CRF}_i \cdot \mathrm{CAPEX}_i(\mathbf{x}) + \mathrm{OPEX}_i(\mathbf{x},\mathbf{y}))$$
$$s.t.\ \mathbf{h}(\mathbf{x},\mathbf{y}) = \mathbf{0}$$
$$\mathbf{g}(\mathbf{x},\mathbf{y}) \leq \mathbf{0}\ .$$

The design variables $\mathbf{x}$ describe the sizing of the individual units; the operation variables $\mathbf{y}$ their operation over the year. The model equations and constraints introduced above are represented in the equality ($\mathbf{h}(\mathbf{x},\mathbf{y})$) and inequality constraints ($\mathbf{g}(\mathbf{x},\mathbf{y})$).

We specify a yearly ammonia production target $\dot{m}_{\mathrm{NH3,y}}$ and ensure meeting this target with an equality constraint $\sum_t \dot{m}_{\mathrm{NH3},t} = \dot{m}_{\mathrm{NH3,y}}$. By specifying this target as an equality constraint, we do not minimize specific costs and avoid division by production rate.

CAPEX is annualized with the capital recovery factor,

$$\mathrm{CRF} = \frac{r \cdot (1+r)^{t_l}}{(1+r)^{t_l} - 1}\ ,$$

with the interest rate r and the lifetime of the respective equipment t_l. For all units, we assume the same interest rate. Because the lifetime of the units differs, we calculate a CRF for every unit. Investment costs are updated to the year 2023 using the chemical engineering plant cost index (CEPCI).

The linear optimization problem is implemented in pyomo [56] and solved using the commercial solver gurobi v12.0.1 [57].

The results are evaluated based on the levelized cost of ammonia LCOA,

$$\mathrm{LCOA} = \frac{\sum_i (\mathrm{CRF}_i \cdot \mathrm{CAPEX}_i + \mathrm{OPEX}_i)}{\sum_t \dot{m}_{\mathrm{NH3},t}}\ ,$$

which is minimized in the optimization. In addition, we evaluate the capacity factor,

$$\mathrm{CF}_{\mathrm{Elec}} = \frac{\sum_t P_{\mathrm{Elec},t}}{P_{\mathrm{Elec,nom}} \cdot t_{\mathrm{op}}}\ ,$$

the electricity consumed by the electrolyzer divided by the electricity consumed when the electrolyzer would be operated at full load for the whole year. The capacity factor describes the electrolyzer's capacity utilization and results from optimal design and operation.

3. Results

First, we analyze the operation of the electrolyzer and energy system without up- and downstream purification to assess the flexibility potential of the eNRR electrolyzer. Second, we integrate the separation processes, and third, we compare the eNRR to the EHB. We consider a medium-sized ammonia production facility with a mean daily ammonia production of 240 $t_{NH3}\ d^{-1}$.

3.1. Optimal design and operation of the electrolyzer

We optimized the design and operation of the eNRR electrolyzer, SP and WP plants, and battery for three operating strategies: direct coupling, curtailment of excess electricity, and battery storage. We investigated three locations: Denmark, with high wind energy potential; Chile, with high solar energy potential; and Australia, with high potential for both wind and solar energy (cf. Table 1). Fig. 3 shows the LCOA and cost contributions of the electrolyzer, SP, WP, and battery storage for the three operating strategies and locations for the year 2023.

LCOA is the lowest for Denmark and the highest for Chile. Denmark has a high capacity factor for WP (cf. Table 1), resulting in consistent and cheap electricity production. This results in a high electrolyzer capacity factor. In Chile, electricity is produced from SP, only, WP availability is low. Because SP is only available during the day, this results in large electrolyzer downtime. This requires a considerably larger electrolyzer oversizing for the same annual ammonia production, resulting in high specific investment costs.

Direct coupling has the highest LCOA in all locations, curtailment reduces LCOA, and battery storage is not economical and thus not applied. The electrolyzer is the main cost contributor in all locations.

Curtailment enables oversizing the SP and WP plants and curtailing electricity peaks when the availability exceeds the nominal load of the electrolyzer. The SP and WP plants are oversized in all locations, resulting in higher electricity availability at off-peak hours and thus a higher capacity factor of the electrolyzer. This higher utilization results in a smaller required electrolyzer capacity for the same annual production, reducing electrolyzer investment costs. As the LCOA is dominated by the electrolyzer cost, reducing these by increasing electricity production costs reduces the LCOA.

The LCOA reduction through curtailment is most pronounced in Australia. Here curtailment enables the hybridization of WP and SP. This can also be seen in the load profile (cf. Figure S3 in the SI). Curtailment increases the mean load of the electrolyzer, and peak electricity production is curtailed. The electrolyzer is operated at full

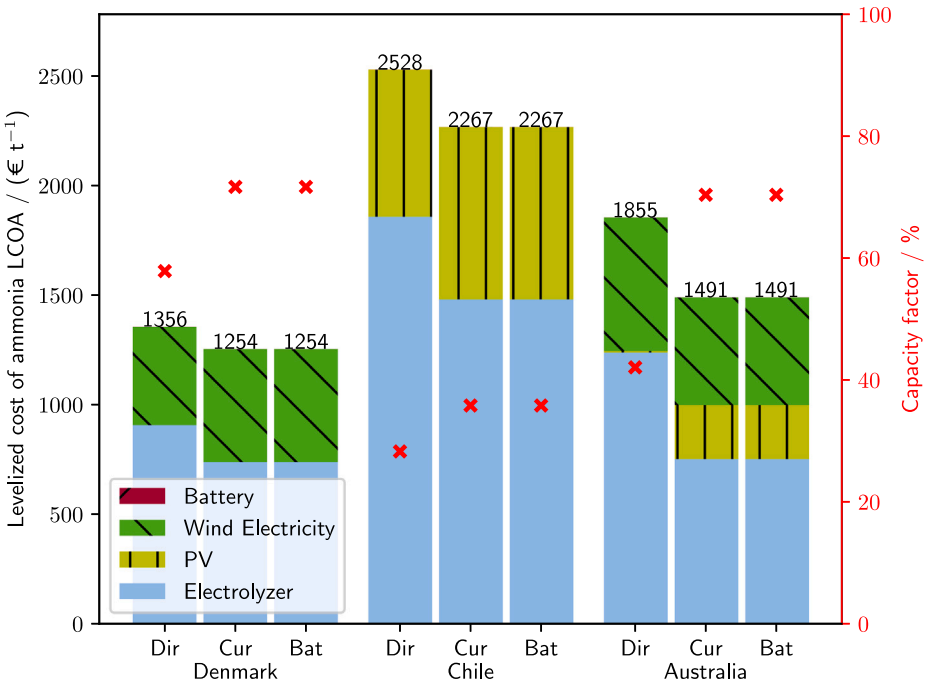


Fig. 3. LCOA and cost contributions of the electrolyzer, WP, SP, and battery storage for the three operating strategies: direct coupling (Dir), curtailment (Cur), and battery storage (Bat) for Denmark, Chile, and Australia for 2023. The red crosses mark the capacity factors of the electrolyzer. Denmark has high a WP and low SP potential, Chile low WP and high SP, Australia high SP and WP.

load for extended durations. The operating profile of Denmark is similar to Australia (cf. Figure S4 in the SI). The effect is limited in Chile because the SP availability is for most time steps either high or zero.

Battery storage promises further cost reduction because electricity peaks could be stored and utilized at times with low electricity availability. However, battery investment costs are too expensive, and implementing no battery results in the lowest costs. Batteries must be installed in sizes similar to the electrolyzer to enable considerable additional ammonia production. When battery costs are considerably reduced (below 200 € kWh^{-1}), it is economically viable to install a small battery in Chile (cf. Figure S8 in the SI). We utilized battery costs from a battery cost projection study by Cole et al. [54]. They forecast battery installation costs for 2035 to be between 147 $ kWh^{-1} to 339 $ kWh^{-1}. Thus, such cost reductions can be expected in the near future.

A considerable amount of hydrogen is produced as a side product and could be sold to improve the process economics. Throughout this analysis, we assume a Faradaic efficiency of 70 %; thus, 30 % of all electrons do not go into ammonia production. We assume that these losses correspond to hydrogen production and thus no further electron losses, such as shunt current or other side products, exist. This results in a hydrogen production of 0.076 $kg_{H2}\,kg_{NH3}^{-1}$.

We calculate the effect of selling this hydrogen by multiplying the production by the revenue of selling hydrogen (selling price minus additional costs for purification and compression) and subtracting it from the LCOA. Because we cannot model the influence of operation conditions on the Faradaic efficiency, annual hydrogen production is constant. Selling hydrogen changes the value of the objective function, but not the optimal design and operation. The LCOA reduction is 76 € t_{NH3}^{-1} for a revenue of 1 € kg_{H2}^{-1} and 152 € t_{NH3}^{-1} for a revenue of 2 € kg_{H2}^{-1}. This highlights the potential of using this side product.

A considerable amount of electricity is wasted if hydrogen cannot be used or sold. However, future work must assess the additional costs for purification and compression. In addition, this work covers off-grid operation in remote locations. The transportation of hydrogen from this remote location will be associated with additional costs; transporting hydrogen is more expensive than transporting ammonia [58].

3.2. Optimal design and operation of the electrolyzer with separation

When considering only the electrolyzer, the eNRR process is flexible and can follow the availability of electricity. This picture changes when nitrogen supply by cryogenic air separation and downstream purification of ammonia by distillation are considered. These processes are constrained by lower load limits and ramp rates. They require electricity during all time steps and constrain the flexible operation of the process

This results in considerably higher LCOA (cf. Fig. 4). The influence of the separation processes far exceeds their investment costs and energy demand. They require operation during times with low to zero availability of electricity. During these times, the electrolyzer will just be turned off. Separation processes, however, must be operated with electricity stored in batteries and material stored in buffer tanks. This results in costly installation of batteries and oversizing of SP and WP. The relative cost increase is similar for all locations and energy supply strategies, ranging from 16 % in Chile to 20 % in Australia. However, the battery cost and the absolute cost increase is the largest for Chile. The pronounced day/night cycle in solar power generation requires larger battery storage size and less stored electricity can be used during intermediate production to power the electrolyzer and to increase ammonia productivity.

The times with zero electricity availability can take up to more than 10 h for the case of Australia (cf. Fig. 5). The longest time with low availability of electricity determines the size and cost of battery storage. During this time, the separation processes must be operated with electricity stored in batteries, and the electrolyzer is turned off.

The energy demand for separation is low compared to that of the electrolyzer and to the battery size. For lithium ion batteries, storage capacity and discharge power are coupled [54]. Thus, the large capacity results in a discharge power greater than that required to operate the separation process. This large discharge power can be seen during the time stamp 3090 h compared to 3178 h (cf. Fig. 5). During the first time stamp, the electricity supply from wind and solar is zero and the battery is discharged at low power to operate the separation. The electrolyzer is turned off. During the second time stamp, the battery is discharged with

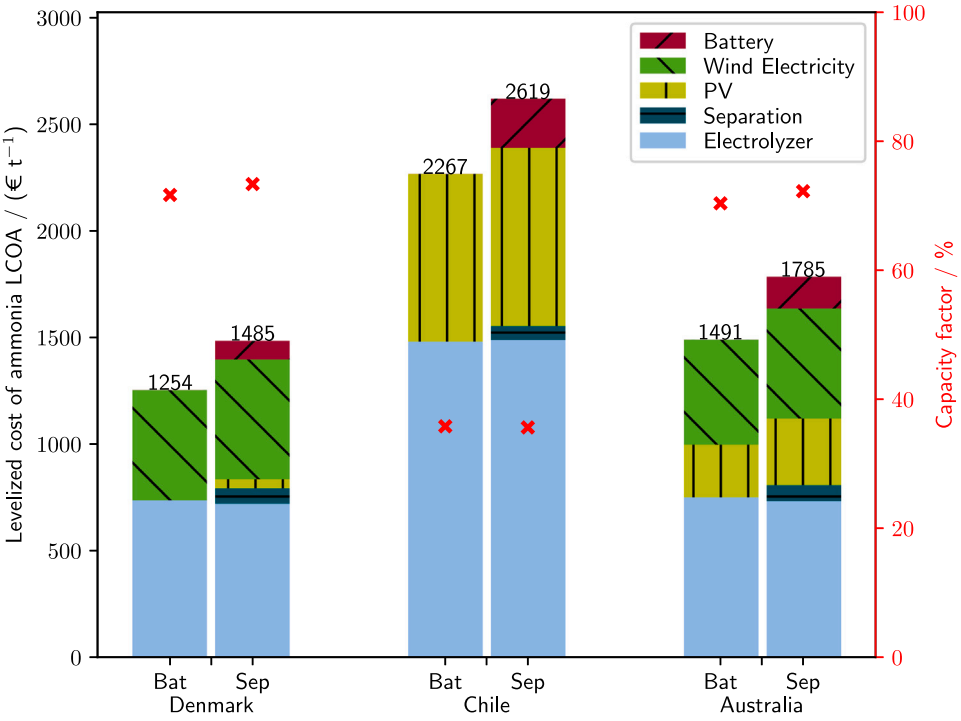


Fig. 4. Comparison of LCOA and cost contributions for electrolyzer operation ignoring separation (Bat) and considering separation (Sep) for 2023. Denmark has high a WP and low SP potential, Chile low WP and high SP, Australia high SP and WP.

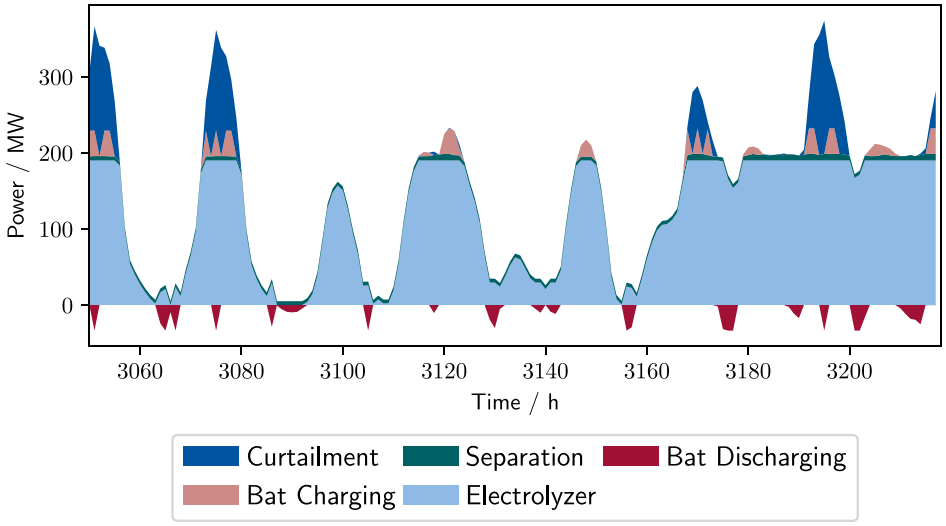


Fig. 5. Operating profile for the separation case study for Australia 2023 for a selected time span of one week. Design and operation were optimized for the whole year. Only electricity consumption and battery discharge are shown.

higher power to operate the electrolyzer during times with high electricity availability. This shows the dual role of the battery. It is used to operate separation processes during low electricity availability, but also to increase electrolyzer productivity during intermediate availability.

Note that repeated charging and discharging during times with excess electricity availability and curtailment can be observed (e.g., at 3075 h). This behavior is equivalent to curtailment and thus a model artifact, because battery efficiency is below 100 % and we do not consider cycle-induced degradation.

We assumed a lower load limit of 50 % of the nominal load for the upstream ASU and 60 % for downstream ammonia purification. The flexibility of nitrogen supply and ammonia separation could be improved by changing the technology, e.g., by utilizing pressure swing adsorption for air separation. We studied the influence of the lower load limit of the separation processes on LCOA by varying their lower load limit individually and combined (cf. Figure S9 in the SI). This sensitivity analysis reveals that the lower load limit of the ammonia separation has a strong influence on LCOA. However, LCOA reduction with increased flexibility shows diminishing returns: LCOA reductions are lower at higher flexibility.

This shows the large influence of the ammonia separation technology and its flexibility. Near-ambient ammonia production, especially in aqueous systems, requires research for efficient and flexible, low-cost separation technologies that can compete with the condensation applied in the HB process. Increasing the flexibility alone will not be sufficient; the energy demand of ammonia separation must be reduced. This could be achieved by changing the technology or increasing the

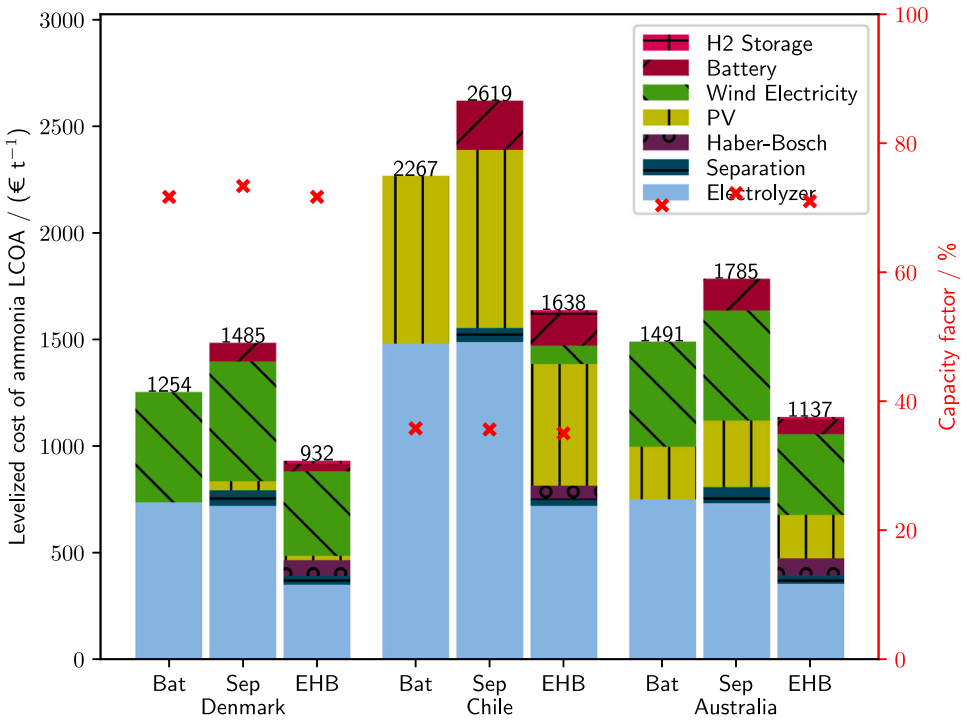


Fig. 6. Comparison of LCOA and cost contributions for the eNRR without (Bat) and with separation (Sep) and the EHB process with water electrolysis (EHB). Denmark has high a WP and low SP potential, Chile low WP and high SP, Australia high SP and WP.

concentration of ammonia in the electrolyzer effluent stream. Changing the ASU technology will have little influence on LCOA.

3.3. Comparison with electrified Haber–Bosch

In the following, we compare the LCOA of the eNRR process (with and without separation) with the EHB process. We optimized the design and operation of the EHB for the three locations introduced above (cf. Table 1). For all locations, the LCOA of the EHB process is about 36 % lower than that of the eNRR (with separation, cf. Fig. 6). The relative cost difference is similar for all locations.

The specific electrolyzer costs of the eNRR are considerably higher. The eNRR current density is 20 times lower than that of PEM water electrolysis. Even though PEM water electrolysis has higher area-specific investment costs, eNRR's lower current density and thus higher electrolyzer area result in considerably higher investment costs. In addition, considerable side product formation in the eNRR further increases required electrolyzer area and energy demand.

The EHB requires additional investment for compressors and high-pressure Haber–Bosch reactors. However, these costs are low compared to those of the electrolyzer and its electricity supply. Thus, LCOA is dominated by the electrolyzer and its energy demand. The high-temperature and high-pressure equipment required for the EHB has little influence on LCOA. This finding on cost contributions is consistent with recent literature (e.g., [19,23]).

The eNRR is more capital intensive due to the higher electrolyzer costs and the higher energy demand. Therefore, it is less suited for flexible operation coupled with intermittent renewable electricity sources. The reduced capacity factor under flexible operation increases specific investment costs. In addition, it leads to higher oversizing of SP and WP and thus to more curtailment to increase the electrolyzer load during intermediate electricity availability. This SP and WP oversizing and curtailment can also be seen when comparing the operating profile (cf. Figure S10 in the SI).

The eNRR has a lower minimal energy demand and avoids the exothermal HB reaction at high temperature and pressure, in which parts of the energy supplied as electricity in the water electrolysis is released as heat. However, its real energy demand is higher as reflected in the higher investment costs for SP and WP. This higher energy demand can be attributed to the side product hydrogen, kinetic limitations of near-ambient nitrogen reduction, and the distillation-based ammonia separation. The distillation has a higher energy demand than the condensation of ammonia in the EHB process. In addition, eNRR's energy demand at minimal load is higher because of the high energy demand and the lower load limit of the separation process.

4. Discussion

The eNRR is considered in the literature to have multiple advantages compared to the EHB, namely a lower energy demand, a lower capital intensity, and a higher flexibility with respect to changes in the energy availability. However, our results show that the LCOA of the eNRR are considerably higher than those of the EHB across all locations and that these theoretical advantages will not realize.

The theoretical minimal energy demand of the eNRR process is lower than that of the EHB; the equilibrium potential at standard conditions of the eNRR is lower than that of the hydrogen evolution. When comparing both process pathways, the difference in energy is released in the exothermic HB reaction.

However, the actual energy demand of the eNRR process is considerably higher ($p_{\mathrm{mean},i}$, cf. Table 2). The main energy consumer of both processes is the electrochemical reaction. Despite the lower equilibrium potential, the operating voltage of the eNRR electrolyzer will be similar to or higher than that of water electrolysis due to the high overpotential of the eNRR [59]. In addition, the FE of the eNRR will be lower because of the formation of side products such as hydrogen. Even if this additional hydrogen can be separated and utilized or sold, this will be associated with additional energy demand and investment costs. A Faradaic efficiency above 90 % is required for the eNRR to have a lower energy demand than EHB [14]. Accounting for separation will further increase this number. Thus, it is expected that the energy demand of the eNRR will always be higher than that of the EHB and that the promise of lower energy demand will not be fulfilled.

Table 2
Mean electricity demand of the eNRR and EHB processes for all locations.

	Denmark	Chile	Australia
$p_{mean,eNRR}$ / kWh kg_{NH3}^{-1}	14.5	14.5	14.5
$p_{mean,EHB}$ / kWh kg_{NH3}^{-1}	10.8	10.7	10.8

A further advantage of the eNRR process mentioned in the literature is a lower capital intensity due to the near-ambient operation. However, for both the eNRR and the EHB processes, the main contribution to CAPEX is the electrolysis and electricity supply for the electrolysis. This finding is in line with the recent eNRR literature (e.g., [7,13]) and EHB (e.g., [19,23]). The eNRR process requires a larger electrolyzer area because the current density will be lower. In addition, the nominal power will be larger because of the side product hydrogen. Thus, the eNRR will require a larger electrolyzer and thus will be more capital-intensive than the EHB process. The high-temperature and high-pressure equipment of the HB step contributes only marginally to the investment costs and energy demand of the EHB (cf. Fig. 6).

Although the findings on the energy demand are true independently of the plant size, the capital intensity changes with scale due to the economies of scale of the HB synthesis loop. The specific costs of the HB loop will increase at small scales for decentralized production, while the specific electrolyzer costs will remain roughly equal. Fernandez et al. [13] and Izelaar et al. [8] showed that distributed small-scale production will significantly increase EHB costs, making eNRR competitive. While it might be true for small scale applications, the EHB will not be built on such a small scale, and such an analysis must also consider production and distribution from larger facilities. In addition, both works did not consider nitrogen supply and ammonia purification, technologies that will also be more expensive on smaller scales.

The eNRR electrolyzer itself is considered to be highly flexible (e.g., [4,7]). However, we show that the flexibility of the complete eNRR process is constrained by separation processes up- and downstream of the electrolyzer. These separation processes have considerably lower energy demand, but limited flexibility. Comparison of eNRR LCOA with and without separation processes shows that they increase LCOA far beyond their investment costs and energy demand because they constrain the flexible operation. The separation processes require additional investments in RES and energy storage to power them during times with low to zero electricity availability (cf. Fig. 5).

In contrast, recent simulation studies on EHB indicate that the HB reactor can be cycled down to as low as 10 % hydrogen load and 50 % energy demand [28]. With this, the flexibility of the EHB is even higher than the flexibility of the eNRR process, also reflected in the low costs of energy storage for the EHB (cf. Fig. 6). Due to the large gap between eNRR and EHB, these conclusions can be drawn on the basis of the simple models applied in this analysis without a detailed flexibility analysis with dynamic models.

Off-grid operation of a process such as the eNRR with one subprocess with high flexibility and high energy demand and one subprocess with low flexibility but low energy demand requires energy storage with large capacity but low discharge power. Cheap energy storage technologies that allow for the individual sizing of capacity and discharge power are better suited for the off-grid operation of the eNRR because they can be tailored to the needs of the process. In the second part of this work, we introduce two energy storage technologies that allow for such decoupled sizing and decrease eNRR LCOA.

The results presented in this work indicate that the theoretical advantages of the eNRR process will not fulfill for large-scale centralized processes. The energy demand of the eNRR is higher because of the lower selectivity of the electrolyzer and the ammonia separation. The LCOA of the eNRR are considerably higher despite the optimistic assumptions on process performance. The flexibility of the eNRR is constrained by the separation processes, the energy demand is higher because of the less efficient electrolyzer and separation, and the CAPEX are higher due to the large electrolyzer.

We performed a sensitivity analysis on model parameters such as Faradaic efficiency, maximum current density, or battery investment costs. Altering model parameters changed the LCOA but the LCOA remained well above the one of the EHB (cf. Figure S11 in the SI). Even further process performance improvements beyond the assumed optimistic electrolyzer performance will not reduce costs below the EHB benchmark. This justifies our findings on the viability of the eNRR for large-scale ammonia production.

For large-scale applications, the EHB process will be more energy efficient and will have a lower LCOA in the short and medium term. As shown in part II of this work, advanced energy storage systems with decoupling of capacity and power can reduce storage costs and thus LCOA but cannot outweigh eNRR's higher electrolyzer costs [15]. When catalysts can be found that combine high Faradaic efficiency and high current density, eNRR might become cost-competitive in the future, as outlined in our previous publication [14]. However, research is far from identifying such a catalyst and we already assumed optimistic future catalyst performance in this study.

5. Conclusion

We evaluated electrochemical nitrogen reduction (eNRR) coupled with intermittent RES (SP and WP) and assessed its viability for off-grid ammonia production. When considering only the electrolyzer and electricity supply, the eNRR process is flexible and can be adjusted to the electricity availability. However, upstream and downstream separation processes that cannot be turned off constrain flexible operation and increase costs far beyond their sheer investment costs and energy demands.

We have shown that the theoretical advantages of the eNRR process cannot be realized even under optimistic assumptions regarding future process performance. The eNRR has considerably higher ammonia production costs than the EHB, even when ignoring separation. This is due to higher electrolyzer costs and higher electricity demand. The electricity demand is higher because of the less efficient electrolysis process (side product hydrogen) and the more energy-intensive separation process. In addition, the minimal electricity demand at part-load operation is higher for eNRR because of the limited flexibility of the ammonia separation.

Studies evaluating the techno-economic potential and the flexible operation of power-to-X processes must also consider energy storage and up- and downstream processes due to their considerable influence on cost and flexibility. Battery storage cannot be tailored to the needs of the eNRR process due to its coupling of capacity and power. In part II of this work, we evaluate how energy storage with decoupled sizing of storage capacity and discharge power can reduce LCOA.

CRediT authorship contribution statement

Michael J. Rix: Writing – review & editing, Writing – original draft, Visualization, Validation, Software, Methodology, Investigation, Formal analysis, Conceptualization. **Judith M. Schwindling:** Writing – review & editing, Software, Investigation. **Karim Bidaoui:** Writing – review & editing, Software, Investigation. **Alexander Mitsos:** Writing – review & editing, Supervision, Methodology, Funding acquisition, Conceptualization.

Declaration of competing interest

The authors declare that they have no known competing financial interests or personal relationships that could have appeared to influence the work reported in this paper.

Acknowledgments

This work has received funding by the European Commission's Horizon Europe project VERGE (no. 101084253) and the HyInnoSep2 project by the Federal Ministry of Research, Technology and Space (BMBF, no. 03ZU2115EA).

Appendix A. Supplementary data

Details on the models and some additional results are given in the document SI.pdf.

Supplementary material related to this article can be found online at https://doi.org/10.1016/j.ijhydene.2026.157496.

References

[1] Appl M. Ammonia: Principles and industrial practice. Weinheim and New York: Wiley-VCH; 2007.
[2] IEA. Ammonia technology roadmap. 2021, https://www.iea.org/reports/ammonia-technology-roadmap.
[3] Smith C, Hill AK, Torrente-Murciano L. Current and future role of Haber–Bosch ammonia in a carbon-free energy landscape. Energy & Environ Sci 2020;13(2):331–44.
[4] MacFarlane DR, Cherepanov PV, Choi J, Suryanto BH, Hodgetts RY, Bakker JM, Ferrero Vallana FM, Simonov AN. A roadmap to the ammonia economy. Joule 2020;4(6):1186–205.
[5] Joseph Sekhar S, Said Ahmed Al-Shahri A, Glivin G, Le TH, Mathimani T. A critical review of the state-of-the-art green ammonia production technologies- mechanism, advancement, challenges, and future potential. Fuel 2024;358:130307.
[6] Wang M, Khan MA, Mohsin I, Wicks J, Ip AH, Sumon KZ, Dinh C-T, Sargent EH, Gates ID, Kibria MG. Can sustainable ammonia synthesis pathways compete with fossil-fuel based Haber–Bosch processes? Energy & Environ Sci 2021;14(5):2535–48.
[7] Hochman G, Goldman AS, Felder FA, Mayer JM, Miller AJM, Holland PL, Goldman LA, Manocha P, Song Z, Aleti S. Potential economic feasibility of direct electrochemical nitrogen reduction as a route to ammonia. ACS Sustain Chem Eng 2020;8(24):8938–48.
[8] Izelaar B, Ramdin M, Vlierboom A, Pérez-Fortes M, van der Slikke D, Sajeev Kumar A, de Jong W, Mulder FM, Kortlever R. Techno-economic assessment of different small-scale electrochemical NH3 production plants. Energy & Environ Sci 2024;17(21):7983–98.
[9] Kim J, Lee S, Choi W, Na J. Toward sustainable ammonia: A techno-economic and environmental assessment of emerging electrochemical ammonia synthesis pathways. Chem Eng J 2025;169131.
[10] Ribeiro C, Santos DMF. Transitioning ammonia production: Green hydrogen-based Haber–Bosch and emerging nitrogen reduction technologies. Clean Technol 2025;7(2):49.
[11] Wu T, Fan W, Zhang Y, Zhang F. Electrochemical synthesis of ammonia: Progress and challenges. Mater Today Phys 2021;16:100310.
[12] Chang B, Zhang H, Sun S, Zhang G. Strategies to achieve effective nitrogen activation. Carbon Energy 2024;e491.
[13] Fernandez CA, Hatzell MC. Editors' choice—economic considerations for low-temperature electrochemical ammonia production: Achieving Haber-Bosch parity. J Electrochem Soc 2020;167(14):143504.
[14] Rix MJ, Mitsos A. Early-stage techno-economic evaluation of electrochemical nitrogen reduction to ammonia based on catalyst performance. Electrochim Acta 2025;145893.
[15] Rix MJ, Lüthje JT, Beles J, Köppen T, Mitsos A. Off-grid electrochemical nitrogen reduction to ammonia II: Energy storage utilizing process streams. Int J Hydrog Energy 2026. submitted for publication.
[16] Schmidhalter I, Mussati MC, Mussati SF, Marcovecchio MG, Aguirre PA. Optimal green ammonia system design for minimum levelized costs in Southern Argentina. Int J Hydrog Energy 2025;121:337–50.
[17] Ikäheimo J, Kiviluoma J, Weiss R, Holttinen H. Power-to-ammonia in future North European 100% renewable power and heat system. Int J Hydrog Energy 2018;43(36):17295–308.
[18] Campion N, Nami H, Swisher PR, Vang Hendriksen P, Münster M. Techno-economic assessment of green ammonia production with different wind and solar potentials. Renew Sustain Energy Rev 2023;173:113057.
[19] Allman A, Daoutidis P. Optimal scheduling for wind-powered ammonia generation: Effects of key design parameters. Chem Eng Res Des 2018;131:5–15.
[20] Kountouris I, Forcellati M, Pantelidis I, Keles D. Renewable hydrogen and ammonia production: Location-specific considerations and competitive market dynamics in Europe. Appl Energy 2025;397:126168.
[21] Liang X, Tang Y, Peng S, Wang X, Tang J, Liu H, Xie J, Zhang H, Ma X. Techno-environmental-economic assessment of green ammonia production system integrated with off-grid offshore wind power. Int J Hydrog Energy 2025;184:151902.
[22] Liu D, Wang Y, Xiong M, Wang Z, Zhou L, He G, Ji X. Capacity configuration and operation scheduling for green ammonia production. Ind Eng Chem Res 2025;64(26):13289–306.
[23] Narciso DA, Pires JM, Fortunato J, Teixeira P, Castro PM, Pinheiro CI, Matos HA. Design and operation of power-to-ammonia systems: A review. Energy Convers Manage 2025;327:119494.
[24] Sass S, Mitsos A. Optimal operation of dynamic (energy) systems: When are quasi-steady models adequate? Comput Chem Eng 2019;124:133–9.
[25] Kopp M, Coleman D, Stiller C, Scheffer K, Aichinger J, Scheppat B. Energiepark mainz: Technical and economic analysis of the worldwide largest power-to-gas plant with pem electrolysis. Int J Hydrog Energy 2017;42(19):13311–20.
[26] Brée LC, Perrey K, Bulan A, Mitsos A. Demand side management and operational mode switching in chlorine production. AIChE J 2019;65(7):e16352.
[27] Caspari A, Tsay C, Mhamdi A, Baldea M, Mitsos A. The integration of scheduling and control: Top-down vs. bottom-up. J Process Control 2020;91:50–62.
[28] Fahr S, Kender R, Bohn J-P, Rehfeldt S, Peschel A, Klein H. Dynamic simulation of a highly load-flexible Haber–Bosch plant. Int J Hydrog Energy 2025;102:1231–42.
[29] Kuckshinrichs W, Ketelaer T, Koj JC. Economic analysis of improved alkaline water electrolysis. Front Energy Res 2017;5:1.
[30] Simoes SG, Catarino J, Picado A, Lopes TF, Di Berardino S, Amorim F, Gírio F, Rangel CM, Ponce de Leão T. Water availability and water usage solutions for electrolysis in hydrogen production. J Clean Prod 2021;315:128124.
[31] Ghobeity A, Mitsos A. Optimal time-dependent operation of seawater reverse osmosis. Desalination 2010;263(1–3):76–88.
[32] Bartman AR, Christofides PD, Cohen Y. Nonlinear model-based control of an experimental reverse-osmosis water desalination system. Ind Eng Chem Res 2009;48(13):6126–36.
[33] Häring H-W, editor. Industrial gases processing. Wiley; 2007.
[34] Klein H, Fritsch P, Haider P, Kender R, Rößler F, Rehfeldt S, Freko P, Hoffmann R, Thomas I, Wunderlich B. Flexible operation of air separation units. ChemBioEng Rev 2021;8(4):357–74.
[35] Schulze JC, Papadimitriou C, Kolmer P, Mitsos A. An integrated scheduling and control scheme with two economic layers for demand side management of chemical processes. AIChE J 2025;71(6):e18731.
[36] Newman J, Balsara NP. Electrochemical systems. The electrochemical society series, 4th ed. Hoboken, NJ: Wiley; 2021.
[37] Pyschik JF, Ebeling KM, Prokopou GI, Rix MJ, Seidenberg JR, Kleiner MB, Leitl M, Mitsos A, Bongartz D. Echerry: A modelica library for modular dynamic modelling of electrochemical reactors. Electrochem Sci Adv 2025;5(3):e202400030.
[38] Varelmann T, Erwes N, Schäfer P, Mitsos A. Simultaneously optimizing bidding strategy in pay-as-bid-markets and production scheduling. Comput Chem Eng 2022;157:107610.
[39] Holst M, Aschbrenner S, Smolinka T, Voglstätter C, Grimm G. Cost forecast for low temperature electrolysis - technology driven bottom-up prognosis for pem and alkaline water electrolysis systems. 2021.
[40] Hemauer J, Rehfeldt S, Klein H, Peschel A. Performance and cost modelling taking into account the uncertainties and sensitivities of current and next-generation pem water electrolysis technology. Int J Hydrog Energy 2023;48(66):25619–34.
[41] Abdel Haleem A, Huyan J, Nagasawa K, Kuroda Y, Nishiki Y, Kato A, Nakai T, Araki T, Mitsushima S. Effects of operation and shutdown parameters and electrode materials on the reverse current phenomenon in alkaline water analyzers. J Power Sources 2022;535:231454.
[42] Zhan G, Cao F, Bai L, Chang F, Zhou B, Duan Y, Zeng S, Dong H, Li Z, Zhang X. Process simulation and optimization of ammonia-containing gas separation and ammonia recovery with ionic liquids. ACS Sustain Chem Eng 2021;9(1):312–25.
[43] Shang D, Zhang X, Zeng S, Jiang K, Gao H, Dong H, Yang Q, Zhang S. Protic ionic liquid [bim][ntf2] with strong hydrogen bond donating ability for highly efficient ammonia absorption. Green Chem 2017;19(4):937–45.
[44] Fan Y, Li Y, Dong X, Hu G, Hua S, Miao J, Zhou D. Extraction of phenols from water with functionalized ionic liquids. Ind Eng Chem Res 2014;53(51):20024–31.
[45] Karami MR, Keshavarz P, Khorram M, Mehdipour M. Analysis of ammonia separation from purge gases in microporous hollow fiber membrane contactors. J Hazard Mater 2013;260:576–84.
[46] Malmali M, Le G, Hendrickson J, Prince J, McCormick AV, Cussler EL. Better absorbents for ammonia separation. ACS Sustain Chem Eng 2018;6(5):6536–46.
[47] Turton R, Bailie RC, Whiting WB, Shaeiwitz JA. Analysis, synthesis and design of chemical processes. Pearson Education; 2008.
[48] Staffell I, Pfenninger S. Using bias-corrected reanalysis to simulate current and future wind power output. Energy 2016;114:1224–39.
[49] Pfenninger S, Staffell I. Long-term patterns of European pv output using 30 years of validated hourly reanalysis and satellite data. Energy 2016;114:1251–65.
[50] S. Pfenninger and I. Staffell. http://www.renewables.ninja. [Accessed 20 October 2025].

[51] Seel Joachim, Kemp Julie Mulvaney, Cheyette Anna, Millstein Dev, Gorman Will, Jeong Seongeun, Robson Dana, Setiawan Rachman, Bolinger Mark. Utility-scale solar, 2024 edition.
[52] Wiser Ryan, Millstein Dev, Hoen Ben, Bolinger Mark, Gorman Will, Rand Joe, Barbose Galen, Cheyette Anna, Darghouth Naïm, Jeong Seongeun, Kemp Julie, O'Shaughnessy Eric, Paulos Ben, Seel Joachim. Land-bases wind market report: 2024 edition.
[53] Vykhodtsev AV, Jang D, Wang Q, Rosehart W, Zareipour H. A review of modelling approaches to characterize lithium-ion battery energy storage systems in techno-economic analyses of power systems. Renew Sustain Energy Rev 2022;166:112584.
[54] Cole W, Ramasamy V, Turan M. Cost projections for utility-scale battery storage: 2025 update.
[55] Morgan ER. Techno-economic feasibility study of ammonia plants powered by offshore wind. 2013.
[56] Bynum ML, Hackebeil GA, Hart WE, Laird CD, Nicholson BL, Siirola JD, Watson J-P, Woodruff DL. Pyomo — Optimization modeling in Python. vol. 67, Cham: Springer International Publishing; 2021.
[57] Gurobi Optimization, LLC. Gurobi optimizer reference manual. 2025.
[58] Schuler J, Ardone A, Fichtner W. A review of shipping cost projections for hydrogen-based energy carriers. Int J Hydrog Energy 2024;49:1497–508.
[59] Abghoui Y, Garden AL, Hlynsson VF, Björgvinsdóttir S, Ólafsdóttir H, Skúlason E. Enabling electrochemical reduction of nitrogen to ammonia at ambient conditions through rational catalyst design. Phys Chem Chem Phys 2015;17(7):4909–18.